Title

Exciton energy transfer reveals spectral signatures of excited states in clusters

Journal

Physical Chemistry Chemical Physics, 22(25)

ISSN

1463-9076

Authors

Lu, Wenchao
Metz, Ricardo B
Troy, Tyler P
et al.

Publication Date

2020-07-01

DOI

10.1039/d0cp02042g

Peer reviewed

Exciton Energy Transfer Reveals Spectral Signatures of Excited States in Clusters

Wenchao Lu,[a] Ricardo B. Metz,*[b] Tyler P. Troy,[a] Oleg Kostko [a] and Musahid Ahmed *[a]

[a.] Chemical Sciences Division, Lawrence Berkeley National Laboratory, Berkeley, CA 94720, USA. Email: mahmed@lbl.gov

[b.] Department of Chemistry, University of Massachusetts, Amherst, Amherst, MA 01003, USA. Email: rbmetz@chem.umass.edu

Abstract:

Electronic excitation and concomitant energy transfer leading to Penning ionization in argon-acetylene clusters generated in a supersonic expansion are investigated with synchrotron-based photoionization mass spectrometry and electronic structure calculations. Spectral features in the photoionization efficiency of the mixed argon-acetylene clusters reveal a blue shift from the $^2P_{1/2}$ and $^2P_{3/2}$ excited states of atomic argon. Analysis of this feature suggests that excited states of argon clusters transfer energy to acetylene results in its ionization and successive evaporation of argon. Theoretically calculated Ar_n (n = 2 – 6) cluster spectra are in excellent agreement with experimental observations, and provide insight into the structure and ionization dynamics of the clusters. A comparison between argon-acetylene and argon-water clusters reveals that argon solvates water better, allowing for higher-order excitons and Rydberg states to be populated. These results are explained by theoretical calculations of respective binding energies and structures.

1. Introduction

The process of Penning ionization, in which an electronically excited atom transfers its energy to an adjacent system that subsequently ionizes originated in the alkali age of chemical reaction dynamics. Elegant experiments, particularly ion momentum spectroscopy with molecular beams,[1, 2] and the advent of tunable synchrotron radiation have revealed these processes in complexes, clusters, and droplets, leading to applications ranging from fundamental spectroscopy to materials science.[3] For instance, it is used in the detection of double neutrino decay in liquid xenon which shows signatures of dark matter.[4] The principle is that gaseous xenon with a dopant such as trimethylamine (TMA) can form composite clusters that convert energy from Xe excitation caused by galactic radiation to ionization of TMA through Penning transfer. A photon of 300 nm wavelength is successively emitted, resulting in the signal being significantly amplified. In other domains of science, excitons in clusters have been investigated for light harvesting in solar energy applications[5, 6] and quantum computing.[7]

It has been known since the 1980s, that pure rare gas clusters can lead to exciton formation with their properties explored explicitly,[3, 8, 9] and that composite rare gas complexes can generate processes reminiscent of Penning ionization.[10, 11] The appeal of using these systems is that a molecular-level picture of energy transfer and ionization could be followed from small clusters hence testable by theory to the bulk material that is relevant for applications. Specifically, molecules embedded or solvated in argon clusters shed light on the dynamics and mechanisms of many chemical and physical processes. For example, Johnson and co-workers have studied the structures of Ar-tagged ion clusters and weak complexes using vibrational predissociation spectroscopy by analyzing and comparing the vibrational bands.[12-15] In a very recent photoelectron spectroscopy study, Lietard et al. used Ar clusters as a model to explore the mechanism of the formation of the self-trapped exciton, which exists in ionic crystals and rare gas matrices.[16] Apart from these spectroscopy studies, Ar clusters were also used to develop new techniques in the realm of physics. For example, Rajeev et al. have reported a technique to accelerate neutral Ar atoms up to mega-eV domain using a laser-plasma accelerator and neutralizer system.[17] The laser pulse first ionizes the Ar clusters, and the ejected electrons sheathe the surrounding neutral Ar clusters, exciting them into a Rydberg state. The excited Ar cluster then becomes a reservoir of electrons, neutralizing the emerging Ar ions via collision, the resulting beam is separated in a Wein filter and is almost fully electrically neutral.

Tunable synchrotron radiation coupled to supersonic molecular beam mass spectrometry provides a universal source for probing molecular clusters whose electronic excitation occurs in the vacuum ultraviolet (VUV) region.[18, 19] Herein, we have chosen to study exciton energy transfer and subsequent ionization dynamics in mixed argon-acetylene clusters. In this work, photoionization efficiency (PIE) curve measurements of the Ar-acetylene cluster ions reveal the electronic excitation from Ar clusters. The excitation spectra of Ar_n (n = 1 – 6) are calculated using equation-of-motion coupled-cluster (EOM-CCSD) theory, and used to fit the PIE measurements of the Ar-C_2H_2 clusters from the experiment. A comparison was made between the current system and a previous Ar-water clusters study[20] to reveal the different solvation and evaporation dynamics at play that may involve excitation to Rydberg states of Ar clusters. The ionization energy (IE) of C_2H_2 (11.4 eV) and the proximity of the vibrational excited states at 11.6 and 11.8 eV[21] correlate to the Ar resonance transitions at 11.62 (^{2}[3/2]°) and 11.83 eV (^{2}[1/2]°),[22, 23] allowing for very efficient energy transfer and subsequent ionization with minimal deposition of internal energy (between 0.2 – 0.4 eV). On the other hand, there is no such correlation in Ar-water clusters, thus resulting in apparent distinctions in both mass spectra and PIE curves between these two systems. The current study allows for a new approach to probe excited states of neutral Ar_n clusters directly which is difficult to attain using traditional absorption spectroscopy in the absence of mass selection. Furthermore, the results may find application in the fields as diverse as microelectronic fabrication via plasmas[24] and the formation of interstellar dust grains[25]. The novel energy transfer pathways seen here, where electronic excitation leads to subsequent ionization in van der Waals bound systems, are reminiscent of Interatomic Coulombic Decay (ICD) processes described by Cederbaum and others[26, 27] and will provide an impetus for new experimental and theoretical time-resolved studies with free-electron lasers and high harmonic generation sources.

2 Experimental and computational

The experiments were performed in a continuous supersonic expansion cluster machine coupled to a three-meter VUV monochromator.[28] During the experiment, 400 Torr of gas mixtures containing 0.1, 1.0, 7.0, 14.0, 30.0, and 100% (by volume) C_2H_2 in Ar were expanded into vacuum through a 50 μm orifice and passed through a 2 mm skimmer. The source chamber was evacuated down to a pressure of 2×10^{-4} Torr. The skimmed beam was intersected perpendicularly with VUV synchrotron radiation between the extraction electrodes of a reflectron time-of-flight mass

spectrometer (RETOF-MS) configured to operate in Wiley-McLaren mode. The time-of-flight (TOF) region was kept at 2×10^{-6} Torr in the second differentially pumped chamber. A start pulse for the TOF was provided by pulsing the repeller plate because of the quasi-continuous (500 MHz) nature of the synchrotron light and investigation of the charged species. Ions thus generated were accelerated vertically to the initial flight path to the field-free RETOF region and detected by a microchannel plate detector. The time-dependent electrical signal from the detector was amplified by a fast preamplifier, collected and digitized by a multichannel scalar card, and then integrated with a computer. Ion counts were measured as a function of synchrotron photon energy from 11 to 15 eV. PIE curves were generated by integrating the ion counts over a mass range of interest for each energy step and normalized by the photon flux.

All the geometry optimization and energetics calculation of $(C_2H_2)Ar_n$ and $(H_2O)_3Ar_n$ (n = 1 – 4) were performed at the ωB97XD/cc-pVTZ level of theory with ultrafine integration grid, using the Gaussian 09 package[29]. The excitation spectra of Ar_1 to Ar_6 clusters were simulated at EOM-CCSD/cc-pVQZ level of theory using Gaussian 09. For comparison, more accurate calculations were done (with the same basis set) using multireference configuration interaction with Davidson correction (MRCI+Q) and spin-orbit coupling correction available in MOLPRO[30, 31]. In these calculations, the cc-pVQZ basis set was uncontracted and augmented, as the "extra" electron in Rydberg states resides in a very large orbital, and describing it correctly requires diffuse functions with smaller exponents than are in the "standard" diffuse basis sets. The three diffuse functions with smallest exponents (ranging from 0.94 to 0.17) were replaced with a set of 6 equally tempered diffuse functions ranging from 1.2 to 0.02. These ranges were chosen based on calculations of Ar atom, where adding more functions with smaller exponents made negligible difference. However, due to the very large size of calculation only up to Ar_3 is available. For Ar_2 and Ar_3, EOM-CCSD and MRCI calculations produce similar results.

3 Results and discussion

3.1 Mass spectra and PIE curve analysis

The mass spectra of five different C_2H_2 to Ar seed ratios recorded at 11.9 eV photon energy (Fig. 1) show that a series of peaks corresponding to C_2H_2 clusters dominate the mass spectra at the concentrations of 7.0% C_2H_2 and above. Another set of peaks corresponding to the C_2H_2 monomer clustered with Ar atoms, $(C_2H_2)Ar_n$, begins to emerge at the 1.0% C_2H_2 concentration and below,

whereas the signal intensities of neat $(C_2H_2)_m$ clusters become negligible. The relative intensities of both neat $(C_2H_2)_m$ and $(C_2H_2)Ar_n$ clusters decrease as the cluster size increases. Fig. 2a shows the PIE curves for $(C_2H_2)Ar_n$ ($n = 1 – 7$), recorded for the 1.0% C_2H_2 mixture. The ionization onset is at 11.26 eV for the $(C_2H_2)Ar$ complex, followed by a plateau and two peaks located at 11.65 and 11.82 eV. The PIE profile of $(C_2H_2)Ar_n$ clusters with $n > 2$ follows a similar trend as the $(C_2H_2)Ar$ cluster. Fig. S1 in the Supplementary Information shows a zoomed-in region between 11.60 and 12.00 eV to better display the spectral shifts. A minor blue shift of 20 meV of each peak per added Ar atom is observed. The grey dashed line shows the PIE for the C_2H_2 monomer with the mid-point value of the onset at 11.40 eV, in good agreement with the PIE spectra from the literature[32, 33] and allowing for absolute calibration of the energy scale. The Ar resonance lines $3p^6 \rightarrow 3p^5 4s$ (J = 1) at 11.62 and 11.83 eV are visible in the PIE of the $(C_2H_2)Ar_n$ clusters.

A scrutiny of the $(C_2H_2)Ar$ cluster PIE curve reveals that the peak at 11.82 eV is a superposition of a sharp peak and a shoulder (Fig. 2b), and changes shape at various C_2H_2 concentrations. To separate the contributions of different components, we analyzed the PIE curves for $(C_2H_2)Ar$ measured at 7.0% C_2H_2 concentration (blue curve) with a negligible contribution of the shoulder component. By subtracting the scaled PIE curve of 7.0% C_2H_2 from the 1.0% mixture, the pure shoulder component in the $(C_2H_2)Ar$ spectrum is thus obtained and shown in a red curve. We first compare the blue curve with the VUV excitation spectra of pure Ar_n clusters which were not mass selected in early studies[34], and find a correlation between the peak at 11.82 eV and the VUV excitation spectrum of Ar_2 (filled cyan peaks). Thus, we denote this component as “dimer component”. The shoulder component correlates to the excitation of a mixture from Ar_3 to Ar_{10} (symbolized as $\overline{Ar_{3\text{-}10}}$) with an average size of Ar_5,[34] and is denoted by “cluster component” (filled magenta peaks). The dissolution of two components also suggests that the broad peak at 11.63 eV results from a superposition of two components. The contribution of the dimer component becomes predominant with an increase of the C_2H_2 concentration, due to smaller Ar_n clusters attached to C_2H_2 in the molecular beam. As seen in Fig. 2b, the strong correlation between the excitation spectra of Ar_2 vs. $\overline{Ar_{3\text{-}10}}$ and the dimer vs. cluster components present in PIE curves of $(C_2H_2)Ar$ suggests that the ionization process of C_2H_2 is essentially caused by the excitation of various-sized Ar_n clusters weakly bound to the surface of the C_2H_2 core. We note here that Kočišek et al. have observed a similar effect on Ar-C_2H_2 clusters using supersonic molecular beam mass spectrometry coupled with electron impact ionization. [35] In their case, they have much larger C_2H_2

clusters binding to Ar, and they invoked a Penning-type mechanism to explain the appearance of ionized Ar-C_2H_2 clusters at around 13.7 eV, correlating to the gas phase Ar (3*d*) excited state. The relationship of the excitation mechanism as a function of cluster size is discussed later in this paper by comparing Ar-C_2H_2 clusters with Ar-H_2O clusters.

3.2 Theoretical fitting

The ionization process of Ar seeded clusters such as Ar-water[20, 36], Ar-benzene[37, 38] and Ar-methanol[39], have been broadly investigated, and the mechanism was widely proposed as Penning ionization, whereas some other studies find resemblance to ICD[40, 41]. During the Penning ionization process, the surface-bound Ar cluster first undergoes $3p^6 \rightarrow 3p^5 4s$ excitation, followed by energy transfer from Ar excitons to the C_2H_2 moiety, causing ionization. Meanwhile, the excess energy is deposited within the cluster and raises the system into a vibrationally excited state. Subsequently, the ionized cluster cools down by evaporating several Ar atoms, which depends on the availability of excess energy after ionization and the kinetic energies of each evaporated Ar atom.

The nature of the Penning ionization mechanism predicts a similarity between the PIE of $(C_2H_2)Ar_n$ and the excitation spectra of pure Ar_n clusters. With this in mind, the excitation spectra of Ar_n (n = 2 – 6) clusters are calculated, which allows for a more insightful comparison. We first calculate the excitation energy for the Ar atom using MRCI+Q with spin-orbit coupling correction coupled with the uncontracted and augmented cc-pVQZ basis set mentioned in the Experimental and Computational section. The calculated excited state energies of the $3s^2 3p^5 4s$ ($^2P_{3/2}$, J = 2, triplet; $^2P_{3/2}$, J = 1, 18% singlet; $^2P_{1/2}$, J = 0, triplet; and $^2P_{1/2}$, J = 1, 82% singlet) states are only about 0.07 eV lower than the reported experimental values.[22] The calculated potential curves of several electronic states of Ar_2 with and without spin-orbit coupling are presented in Fig. 3a and 3b. For clarity, only spin-orbit states with $\Omega = 0_u^+$ and 1_u are shown, as only these states have allowed electronic transitions from the $\Omega = 0_g^+$ ground state. Some excited states are repulsive, while others have a deep potential well, as they are Rydberg states that correlate to $Ar_2^+ + e^-$. However, this potential well appears at small r(Ar-Ar), resulting in very little Franck-Condon overlap with the ground state, which has a bond length of 4.0 Å and a very flat potential leading to a very broad v = 0 wave function. These calculations agree with previous results of the ground and $^1\Sigma_u^+$ states at the CCSR(3) level without spin-orbit coupling.[42] The EOM-CCSD and MRCI+Q calculated spectra show two peaks, corresponding to transitions to the $^1\Sigma$ (lower energy) and $^1\Pi$

(higher energy) states. The addition of spin-orbit coupling splits some of the states, especially those from Σ states, and the $\Omega = 0_u^+$ components of the $^1\Sigma_u^+$ and $^3\Pi_u$ states show an avoided crossing (Fig. 3b). The calculated spectrum with spin-orbit coupling (Fig. 3c) relates very well to that obtained from the experiment.[34] For Ar_3, the simulated spectra at MRCI+Q with and without spin-orbit coupling are shown in Fig. 3d. Here only one global minimum geometry, an equilateral triangle at *r*(Ar-Ar) = 4.0 Å, is considered. The resolution is set to 50 meV Gaussian linewidth, based on our experimental conditions. The EOM-CCSD and MRCI calculations give similar results, and the addition of spin-orbit splitting has little effect on the high-energy peak (from Π states) but splits the low-energy peak (from Σ states), which is very similar to the scenario for Ar_2.

The evolution of the spectrum with cluster size is calculated using the EOM-CCSD level of theory as a compromise between accuracy and reduced computation time. Based on the potential curve calculated along *r*(Ar-Ar), the structures of Ar_n (n = 3 – 6) cluster are generated with all nearest neighboring *r*(Ar-Ar) at 4.0 Å, and only the single geometry with the highest symmetry (and lowest energy)[43] is considered for each spectrum. This is a tetrahedral geometry for Ar_4 and trigonal bipyramidal for Ar_5. Other structural isomers may exist in the molecular beam, such as square planar Ar_4 and square pyramidal Ar_5, which are calculated to be 9.4 and 4.2 meV higher in energy than the lowest energy conformers, respectively, at the CCSD level with the augmented and uncontracted cc-pVQZ basis set. Fig. 4a compares the spectra of the tetrahedral and square planar Ar_4 isomers, indicating that the low-energy peak barely shifts, whereas the high-energy peak shifts by 0.05 eV. A similar trend is observed between the trigonal bipyramidal and square pyramidal Ar_5 isomers, as the low-energy peak barely shifts and the high-energy peak shifts by only 0.03 eV. Therefore, the influence caused by structural isomerization is ignored when generating the excitation spectra of Ar_n (n = 1 – 7) clusters. As seen in Fig. 3e, the lower-energy peak blue shifts by 35 meV for each additional Ar whereas the higher-energy peak shifts by 50 meV. These findings correlate very well with what we observe in PIE measurements of $(C_2H_2)Ar_n$ with a 20 – 40 meV blue shift per added Ar atom (Fig. 2a and Fig. S1). Such blue shifts observed experimentally and verified theoretically support our hypothesis of a Penning-ionization type mechanism. Since each $(C_2H_2)Ar_n$ PIE spectrum may appear as a superposition of several Ar_n spectra, we tentatively fit those PIE curves with the abovementioned EOM-CCSD calculated Ar_n spectra. The results are shown in Fig. 5. The fitting of the experimental $\overline{Ar_{3\text{-}10}}$ spectrum shows a predominant contribution of Ar_5 (Fig. 5a), consistent with the average cluster size of the previous

studies using fluorescence detection.[34] There is also a possible contribution from $Ar_{7\text{-}10}$ (not included in the fit) that would assist to fill in the region near 12.0 eV. The fitting from EOM-CCSD calculated Ar_n spectra can simulate the peak position and profile around 11.93 eV (Π states), but fails to reproduce the peak at 11.70 eV (Σ states) due to the omission of spin-orbit coupling. Successively, the fitting of the PIE curves of $(C_2H_2)Ar_n$ (n = 1 – 3) is presented in Fig. 5b – d. We note that as n in $(C_2H_2)Ar_n$ becomes larger, the dominant Ar_n spectrum follows the same trend but is slightly larger than in the corresponding Ar_n cluster, as Ar_3 has the highest population for fitting the PIE of $(C_2H_2)Ar$. This is probably because extra Ar atoms evaporate after ionization, leading to the convergence to the final observed smaller species. Also, the aforementioned dimer contribution that mainly comes from Ar and Ar_2 gradually diminishes with larger n. The PIE curves of $(C_2H_2)Ar_n$ to some extent reflect the excitation spectra of Ar_n clusters with a relatively narrow size distribution, and allow for a new approach to probe excited states of neutral Ar_n clusters directly.

3.3 A comparison to the Ar-water system

We have previously studied the Ar-mediated ionization of water seeded clusters using similar techniques.[20] In this system, the most prominent peak is the water tetramer $(H_2O)_4^+$ and its protonated counterpart $(H_2O)_4H^+$. Experimentally, the ratio of the two gaseous components are comparable between the Ar-C_2H_2 and Ar-H_2O, but the expansion conditions are different, as the backing pressure for Ar-H_2O clusters is roughly 3.5 times higher (5250 Torr) than that of Ar-C_2H_2. We use scaling laws to determine the number of bound argon atoms, and postulate that the core C_2H_2 holds around 10 Ar atoms whereas the water cluster is bound with 20 Ar atoms.[34, 44] A noticeable difference, however, is that in comparison with abundant $(C_2H_2)Ar_n$ signals, the Ar mediated counterparts for water ($(H_2O)_m^+Ar_n$ and $(H_2O)_mH^+Ar_n$) are missing with only bare water and protonated water clusters observed.

To investigate the missing signal of $(H_2O)_m^+Ar_n$ and $(H_2O)_mH^+Ar_n$, we first compared the IE of $(H_2O)_m$ and C_2H_2. For $(H_2O)_m$ clusters, the appearance energies (the upper limit to the adiabatic IE) are reported to lie beneath 11.15 eV for $(H_2O)_3$, and then decrease with the increasing water cluster size and gradually converge to 10.6 eV.[28] For comparison, the IE threshold for C_2H_2 monomer is 11.35 eV. This indicates that for the Ar-H_2O clusters, following ionization of the core $(H_2O)_m$, there is at least 0.2 eV of excess energy available to cause evaporation of Ar from the cluster. From an energetic perspective, the binding energy E_{bind} of each Ar atom attached is

calculated as:

$$E_{bind} = E[(X)Ar_n] - E[(X)Ar_{n-1}] - E[Ar],$$

where E is the electronic energy with zero-point correction at ωB97XD/cc-pVTZ level of theory, and X is either C_2H_2 or $(H_2O)_3$. Here, $(H_2O)_3$ is chosen as the model system to mimic the water cluster core, since the cluster size m = 3 is the onset showing a cluster like property rather than individual water molecule and significantly lowers the IE.[28] The E_{bind} of the first Ar attached to C_2H_2 is calculated to be 10 meV, which correlates quite well with our benchmark CBS-QB3 value of 9 meV. The binding energies of both $(C_2H_2)Ar_n$ and $(H_2O)_3Ar_n$ lie within the same magnitude, converging to ~ 30 meV as the cluster size increases (Table 1). Thus, the excess energy available upon ionization of the water cluster is sufficient to evaporate at least 7 more Ar atoms. The evaporation of Ar renders the PIE profile of Ar-bound $(H_2O)_m$ to be dominated by the "cluster component", in contrast to that of $(C_2H_2)Ar$ as shown in Fig. 2b. In $(C_2H_2)Ar_n$, the excitations of Ar $3p^6 \rightarrow 3p^5 4s$ (11.62 and 11.83 eV) coincide with two vibrationally excited states of $C_2H_2^+$, as noted in Fig. 2a, but for the Ar-H_2O system there is no such coincidence. We postulate that this coincidence may allow the transfer of vibrational energy from $C_2H_2^+$ being less efficient and non-statistical, as the excess energy after ionization of the C_2H_2 may have little time for the Ar atoms to redistribute. Some energy is confined within the $C_2H_2^+$ (the C-C stretch is 1818 cm^{-1} = 0.225 eV), which leads to even less energy available for driving off attached Ar atoms.

Previous studies have observed three types of excitation bands in the excitation spectra of Ar_n: surface-type excitation, bulk excitation and excitation from Rydberg states.[45-47] The peaks from 11.6 – 12.2 eV in the PIE curves of $(C_2H_2)Ar_n$ discussed above mainly correlate to surface-type excitation with the main quantum number n = 1 and 1' (Frenkel-type excitons) of pure Ar_n clusters. These excitons are usually from tightly bound states localized at one atom, showing a relatively smaller radius and higher electron binding energy. Above 13.0 eV, a broad continuum is observed with less pronounced intensity and is assigned as the excitation to overlapping Rydberg states with wave functions extending beyond the radius of the cluster. Apart from the broad continuum, some minor peaks exist around 13.5 – 15.0 eV and entangle with the Rydberg states. These peaks correlate to the bulk excitation (Wannier excitons, n = 2 – 4) with a radius larger than the lattice spacing and smaller electron binding energy due to the weakened Coulomb interaction between electron and hole.

A comparison of the PIE curves for $(C_2H_2)Ar$ and protonated $(H_2O)_4$ all from dilute expansions

in Ar is shown in Fig. 6, together with the excitation spectrum of Ar_{15} from the work of Wörmer et al.[48] The PIE profile for the Ar-H_2O system is similar to the "cluster component" of $(C_2H_2)Ar$, with the peak position around 11.92 eV. The assignment of Ar_{15} spectrum shows that the peak around 11.92 eV is composed of n = 1' (main quantum number) surface-type excitation and n = 1 bulk excitation.[46, 48] The PIE curve of $(H_2O)_4H^+$ correlates well with the excitation spectrum of Ar_{15}, especially in the region above 13.0 eV that contains the contributions from Rydberg states, indicating the size of Ar_n cluster seeded together with the structure being similar to Ar_{15}. A careful examination in the Rydberg excitation region above 13 eV shows some minor differences between $(H_2O)_4H^+$ and $(C_2H_2)Ar^+$. By normalizing the $(C_2H_2)Ar^+$ curve from 12.5 – 13.0 eV with the $(H_2O)_4H^+$ curve, we observe the excitation band between 13.0 – 14.0 eV appears strongly in the $(H_2O)_4H^+$ curve, corresponding to the n = 2 and 2' surface excitons of solid Ar as observed in earlier studies.[34, 48] Another excitation band appears around 14.4 eV, probably associated with higher bulk excitation (Wannier exciton) that only becomes significant for larger Ar_n (n > 15) clusters.[46, 48] This indicates that the nascent $(H_2O)_mAr_n$ clusters produced from supersonic expansion are attached with more Ar atoms and solvated better compared with $(C_2H_2)Ar_n$ clusters, which is in good agreement with our experimental conditions.

We optimized the geometries for $(C_2H_2)Ar_n$ and $(H_2O)_3Ar_n$ (n = 1 – 4, Fig. 7). The average calculated r(Ar-Ar) is around 4.15 – 4.20 Å, with all the Ar atoms wrapping around the core C_2H_2 or $(H_2O)_3$. Alkan et al. have calculated the structures of pure Ar_n clusters (n = 3 – 10) using various levels of theory.[43] The reported global minimum of each cluster exhibits a highly symmetrical structure and a sterically compact stacking pattern. Borges et al. have further calculated the structures of $(H_2O)Ar_n$ (n = 1 – 26), and found that as the cluster size increases, the Ar atoms prefer to stack alongside the oxygen of H_2O asymmetrically until the central H_2O is completely solvated when $n \geq 12$.[49] It is reasonable to deduce that more Ar atoms are required to completely encapsulate the larger $(H_2O)_n$ clusters, compared with the relatively smaller C_2H_2 core, and such differentiation in the stacking pattern may account for the origin of discrepancies in Rydberg states between $(C_2H_2)Ar_n$ and $(H_2O)_mAr_n$. Also, the compact stacking of the Ar is not predicted in our calculations, especially for n = 4, which exhibits a rhomboid stacking of the Ar atoms instead of a tetrahedron. We suspect that this stacking pattern reduces the Ar-Ar dispersion, but is counterbalanced by increased dispersion interaction between Ar and C_2H_2, and facilitates surface-type excitation rather than bulk excitation that usually happens in the interior of the cluster.

4 Conclusion

We have investigated the photoionization of gas-phase Ar-acetylene clusters using VUV radiation coupled to supersonic molecular beam mass spectrometry. $(C_2H_2)Ar_n$ clusters have been observed, and their PIE curves have been measured. The resemblance between the appearances of PIE curves with the excitation spectra of Ar_n clusters is explained by Penning ionization. The PIE curves can be fitted with the EOM-CCSD calculated excitation spectra of Ar_n clusters. A slight blue shift for the Ar excited states is noticed as the size of Ar_n cluster size increases, which is reproducible from calculations. A comparison has been made with a previous Ar-water study using similar techniques. Unlike the Ar-C_2H_2 cluster system, no $(H_2O)_mAr_n$ peaks are observed due to the lower ionization energy of water clusters making more excess energy available upon ionization, which leads to evaporation of Ar. A comparison of their PIE curves reveals that the peak position around 11.92 eV of $(H_2O)_4H^+$ resembles the cluster component of $(C_2H_2)Ar$, and the 13.0 – 14.0 eV region of $(H_2O)_4H^+$ shows more excitation from Rydberg states arising from larger Ar_n clusters.

Conflicts of interest

There are no conflicts to declare.

Acknowledgments

This work is supported by the Director, Office of Science, Office of Basic Energy Sciences, of the U.S. Department of Energy under Contract No. DE-AC02-05CH11231, through the Gas Phase Chemical Physics Program, Chemical Sciences Division. The Advanced Light Source is supported by the same contract. RM acknowledges support from the National Science Foundation under Award No. CHE-1856490. The MOLPRO calculations were carried out at the National Energy Research Scientific Computing Center, a DOE Office of Science User Facility supported by the Office of Science of the U.S. Department of Energy under Contract No. DE-AC02-05CH11231.

References

1. J. Ullrich, R. Moshammer, R. Dörner, O. Jagutzki, V. Mergel, H. Schmidt-Böcking and L. Spielberger, *J. Phys. B*, 1997, **30**, 2917-2974.
2. S. Marburger, O. Kugeler, U. Hergenhahn and T. Möller, *Phys. Rev. Lett.*, 2003, **90**, 203401.

3. C. Bostedt, T. Gorkhover, D. Rupp and T. Möller, in *Synchrotron Light Sources and Free-Electron Lasers: Accele-rator Physics, Instrumentation and Science Applications*, Springer International Publishing, Cham, 2019, pp. 1-49.
4. Y. Nakajima, A. Goldschmidt, H. S. Matis, D. Nygren, C. Oliveira and J. Renner, *J. Phys. Conf. Ser.*, 2015, **650**, 012012.
5. B. A. Gregg, *J. Phys. Chem. B*, 2003, **107**, 4688-4698.
6. G. P. Rutkowski and B. A. Grimes, *ACS Appl. Energy Mater.*, 2019, **2**, 6311-6321.
7. T. Heindel, A. Thoma, I. Schwartz, E. R. Schmidgall, L. Gantz, D. Cogan, M. Strauß, P. Schnauber, M. Gschrey, J.-H. Schulze, A. Strittmatter, S. Rodt, D. Gershoni and S. Reitzenstein, *APL Photonics*, 2017, **2**, 121303.
8. C. J. Bardeen, *Annu. Rev. Phys. Chem.*, 2014, **65**, 127-148.
9. G. D. Scholes, *Faraday Discuss.*, 2020, **221**, 265-280.
10. Ö. Şahin, İ. Tapan, E. N. Özmutlu and R. Veenhof, *JINST*, 2010, **5**, P05002-P05002.
11. S. Falcinelli, F. Pirani, P. Candori, B. G. Brunetti, J. M. Farrar and F. Vecchiocattivi, *Front. Chem.*, 2019, **7**.
12. J. C. Bopp, E. G. Diken, J. M. Headrick, J. R. Roscioli, M. A. Johnson, A. J. Midey and A. A. Viggiano, *J. Chem. Phys.*, 2006, **124**, 174302.
13. L. R. McCunn, J. R. Roscioli, M. A. Johnson and A. B. McCoy, *J. Phys. Chem. B*, 2008, **112**, 321-327.
14. H. K. Gerardi, G. H. Gardenier, U. Viswanathan, S. M. Auerbach and M. A. Johnson, *Chem. Phys. Lett.*, 2011, **501**, 172-178.
15. R. A. Relph, B. M. Elliott, G. H. Weddle, M. A. Johnson, J. Ding and K. D. Jordan, *J. Phys. Chem. A*, 2009, **113**, 975-981.
16. A. Lietard, G. Piani, M. Briant, M.-A. Gaveau, S. Faisan, V. Mazet, B. Soep, J.-M. Mestdagh and L. Poisson, *Phys. Chem. Chem. Phys.*, 2018, **20**, 11206-11214.
17. R. Rajeev, T. Madhu Trivikram, K. P. M. Rishad, V. Narayanan, E. Krishnakumar and M. Krishnamurthy, *Nat. Phys.*, 2013, **9**, 185.
18. O. Kostko, B. Bandyopadhyay and M. Ahmed, *Annu. Rev. Phys. Chem.*, 2016, **67**, 19-40.
19. M. Ahmed and O. Kostko, *Phys. Chem. Chem. Phys.*, 2020, **22**, 2713-2737.
20. A. Golan and M. Ahmed, *J. Phys. Chem. Lett.*, 2012, **3**, 458-462.
21. P. Plessis and P. Marmet, *Int. J. Mass Spectrom. Ion Processes*, 1986, **70**, 23-44.

22. L. Minnhagen, *J. Opt. Soc. Am.*, 1973, **63**, 1185-1198.
23. I. Velchev, W. Hogervorst and W. Ubachs, *J. Phys. B*, 1999, **32**, L511.
24. D. B. Graves, *AlChE J.*, 1989, **35**, 1-29.
25. T. Stein, B. Bandyopadhyay, T. P. Troy, Y. Fang, O. Kostko, M. Ahmed and M. Head-Gordon, *PNAS*, 2017, **114**, E4125-E4133.
26. L. S. Cederbaum, J. Zobeley and F. Tarantelli, *Phys. Rev. Lett.*, 1997, **79**, 4778-4781.
27. T. Jahnke, *J. Phys. B*, 2015, **48**, 082001.
28. L. Belau, K. R. Wilson, S. R. Leone and M. Ahmed, *J. Phys. Chem. A*, 2007, **111**, 10075-10083.
29. M. J. Frisch, G. W. Trucks, H. B. Schlegel, G. E. Scuseria, M. A. Robb, J. R. Cheeseman, G. Scalmani, V. Barone, B. Mennucci, G. A. Petersson, H. Nakatsuji, M. Caricato, X. Li, H. P. Hratchian, A. F. Izmaylov, J. Bloino, G. Zheng, J. L. Sonnenberg, M. Hada, M. Ehara, K. Toyota, R. Fukuda, J. Hasegawa, M. Ishida, T. Nakajima, Y. Honda, O. Kitao, H. Nakai, T. Vreven, J. J. A. Montgomery, J. E. Peralta, F. Ogliaro, M. Bearpark, J. J. Heyd, E. Brothers, K. N. Kudin, V. N. Staroverov, T. Keith, R. Kobayashi, J. Normand, K. Raghavachari, A. Rendell, J. C. Burant, S. S. Iyengar, J. Tomasi, M. Cossi, N. Rega, J. M. Millam, M. Klene, J. E. Knox, J. B. Cross, V. Bakken, C. Adamo, J. Jaramillo, R. Gomperts, R. E. Stratmann, O. Yazyev, A. J. Austin, R. Cammi, C. Pomelli, J. W. Ochterski, R. L. Martin, K. Morokuma, V. G. Zakrzewski, G. A. Voth, P. Salvador, J. J. Dannenberg, S. Dapprich, A. D. Daniels, O. Farkas, J. B. Foresman, J. V. Ortiz, J. Cioslowski and D. J. Fox, *Gaussian 09, Revision C.01, Gaussian, Inc., Wallingford CT, 2010.*
30. H. J. Werner, P. J. Knowles, G. Knizia, F. R. Manby and M. Schütz, *WIREs Comput. Mol. Sci.*, 2012, **2**, 242-253.
31. H. J. Werner, P. J. Knowles, G. Knizia, F. R. Manby, M. Schütz, P. Celani, W. Györffy, D. Kats, T. Korona, R. Lindh, A. Mitrushenkov, G. Rauhut, K. R. Shamasundar, T. B. Adler, R. D. Amos, A. Bernhardsson, A. Berning, D. L. Cooper, M. J. O. Deegan, A. J. Dobbyn, F. Eckert, E. Goll, C. Hampel, A. Hesselmann, G. Hetzer, T. Hrenar, G. Jansen, C. Köppl, Y. Liu, A. W. Lloyd, R. A. Mata, A. J. May, S. J. McNicholas, W. Meyer, M. E. Mura, A. Nicklass, D. P. O'Neill, P. Palmieri, D. Peng, K. Pflüger, R. Pitzer, M. Reiher, T. Shiozaki, H. Stoll, A. J. Stone, R. Tarroni, T. Thorsteinsson and M. Wang, *MOLPRO, version 2015.1, a package of ab initio programs*, Cardiff, UK, 2015.

32. V. H. Dibeler and R. M. Reese, *J. Res. Natl. Bur. Std.*, 1964, **68A**, 409-423.
33. A. J. C. Nicholson, *J. Chem. Phys.*, 1965, **43**, 1171-1177.
34. J. Wörmer, V. Guzielski, J. Stapelfeldt, G. Zimmerer and T. Möller, *Phys. Scr.*, 1990, **41**, 490-494.
35. J. Kočišek, J. Lengyel and M. Fárník, *J. Chem. Phys.*, 2013, **138**, 124306.
36. J. Kočišek, J. Lengyel, M. Fárník and P. Slavíček, *J. Chem. Phys.*, 2013, **139**, 214308.
37. W. Kamke, B. Kamke, H. U. Kiefl, Z. Wang and I. V. Hertel, *Chem. Phys. Lett.*, 1986, **128**, 399-403.
38. B. Kamke, W. Kamke, Z. Wang, E. Rühl and B. Brutschy, *J. Chem. Phys.*, 1987, **86**, 2525-2529.
39. G. Vaidyanathan, M. T. Coolbaugh, W. R. Peifer and J. F. Garvey, *J. Chem. Phys.*, 1991, **94**, 1850-1858.
40. M. Mucke, M. Braune, S. Barth, M. Förstel, T. Lischke, V. Ulrich, T. Arion, U. Becker, A. Bradshaw and U. Hergenhahn, *Nat. Phys.*, 2010, **6**, 143-146.
41. T. Jahnke, H. Sann, T. Havermeier, K. Kreidi, C. Stuck, M. Meckel, M. Schöffler, N. Neumann, R. Wallauer, S. Voss, A. Czasch, O. Jagutzki, A. Malakzadeh, F. Afaneh, T. Weber, H. Schmidt-Böcking and R. Dörner, *Nat. Phys.*, 2010, **6**, 139-142.
42. B. Fernández and H. Koch, *J. Chem. Phys.*, 1998, **109**, 10255-10262.
43. M. Alkan, P. Xu and M. S. Gordon, *J. Phys. Chem. A*, 2019, **123**, 8406-8416.
44. O. F. Hagena, *Z. Phys. D*, 1987, **4**, 291-299.
45. F. Carnovale, J. B. Peel, R. G. Rothwell, J. Valldorf and P. J. Kuntz, *J. Chem. Phys.*, 1989, **90**, 1452-1459.
46. J. Wörmer, R. Karnbach, M. Joppien and T. Möller, *J. Chem. Phys.*, 1996, **104**, 8269-8278.
47. F. Merkt and H. Schmutz, *J. Chem. Phys.*, 1998, **108**, 10033-10045.
48. J. Wörmer, M. Joppien, G. Zimmerer and T. Möller, *Phys. Rev. Lett.*, 1991, **67**, 2053-2056.
49. E. Borges, G. G. Ferreira and J. P. Braga, *Int. J. Quantum Chem.*, 2008, 108, 2523-2529.

Table 1 The binding energy of the *n*th Ar (n = 1 – 4) attached to $(C_2H_2)Ar_n$ and $(H_2O)_3Ar_n$ clusters. The values are calculated under ωB97XD/cc-pVTZ level of theory and presented in meV.

	E_{bind} (meV)			
	***n* = 1**	***n* = 2**	***n* = 3**	***n* = 4**
$(C_2H_2)Ar_n$	9.5	14.3	25.9	24.7
$(H_2O)_3Ar_n$	24.7	27.1	28.8	30.9

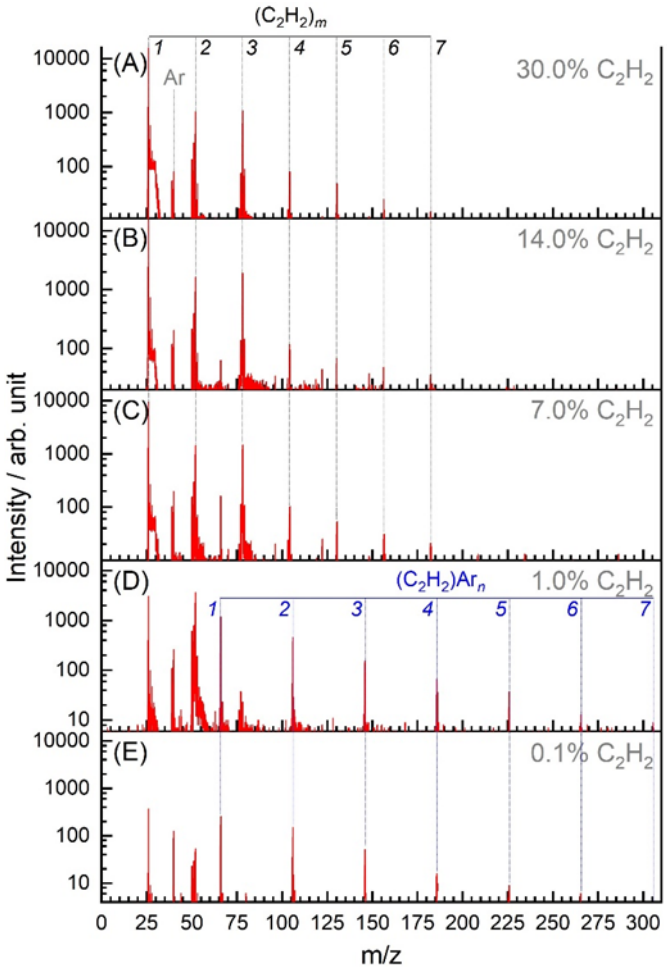

Fig. 1 Mass spectra of reactant gas mixture containing: (A) 30.0%, (B) 14.0%, (C) 7.0%, (D) 1.0% and (E) 0.1% of C_2H_2 in Ar, recorded at 11.9 eV VUV photon energy. The peaks of clusters $(C_2H_2)_m$ (m = 1 – 7) and acetylene seeded Ar clusters, $(C_2H_2)Ar_n$ (n = 1 – 7) are cross-labelled.

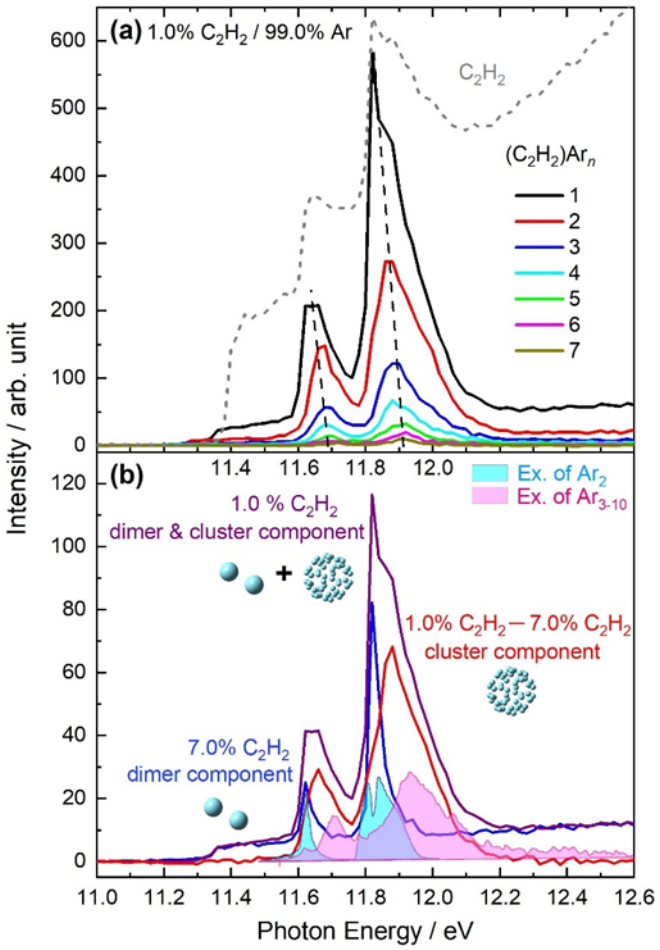

Fig. 2 (a) The PIE curves of $(C_2H_2)Ar_n$ (n = 1 – 7) at the concentration of 1.0% C_2H_2 in Ar. The grey dashed line indicates the PIE curve for pure C_2H_2; and (b) the PIE curve of pure "cluster component" for $(C_2H_2)Ar$ (red), obtained by scaling and subtracting the PIE curve of $(C_2H_2)Ar$ for 7% C_2H_2 concentration (blue, containing "dimer component" only) from the 1.0% mixture (purple). The excitation spectra of Ar_2 (cyan) and $\overline{Ar_{3\text{-}10}}$ (magenta) from Ref. 34 are also shown for comparison.

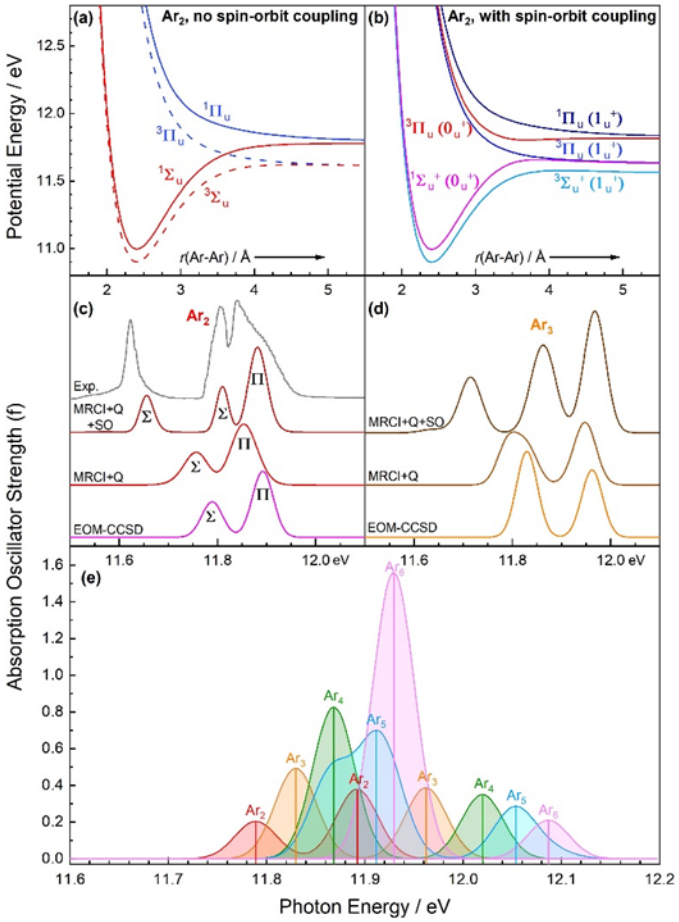

Fig. 3 The MRCI+Q calculated potential energy curves for some excited states of Ar_2, without (a) and with spin-orbit coupling (b); the calculated Ar_2, (including experimental spectrum adapted from Ref. 34, c) and Ar_3 (d) excitation spectra corresponding to the transition $3p^6 \rightarrow 3p^5 4s$, using EOM-CCSD, MRCI+Q and MRCI+Q+SO methods; and (e) excitation spectra of $Ar_{2\text{-}6}$ clusters calculated at the EOM-CCSD level of theory.

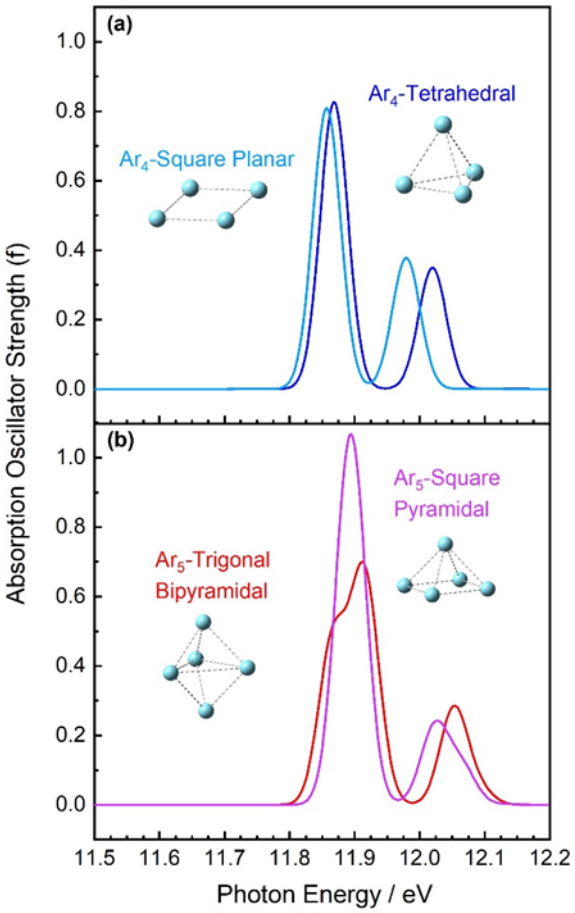

Fig. 4 The calculated excitation spectra of (a) tetrahedral and square planar Ar_4 isomers, and (b) trigonal bipyramidal and square pyramidal Ar_5 isomers. All spectra are generated based on all the nearest neighboring *r*(Ar-Ar) being 4.0 Å, and calculated at the EOM-CCSD level of theory. The spectra have been convoluted with 40 meV Gaussians.

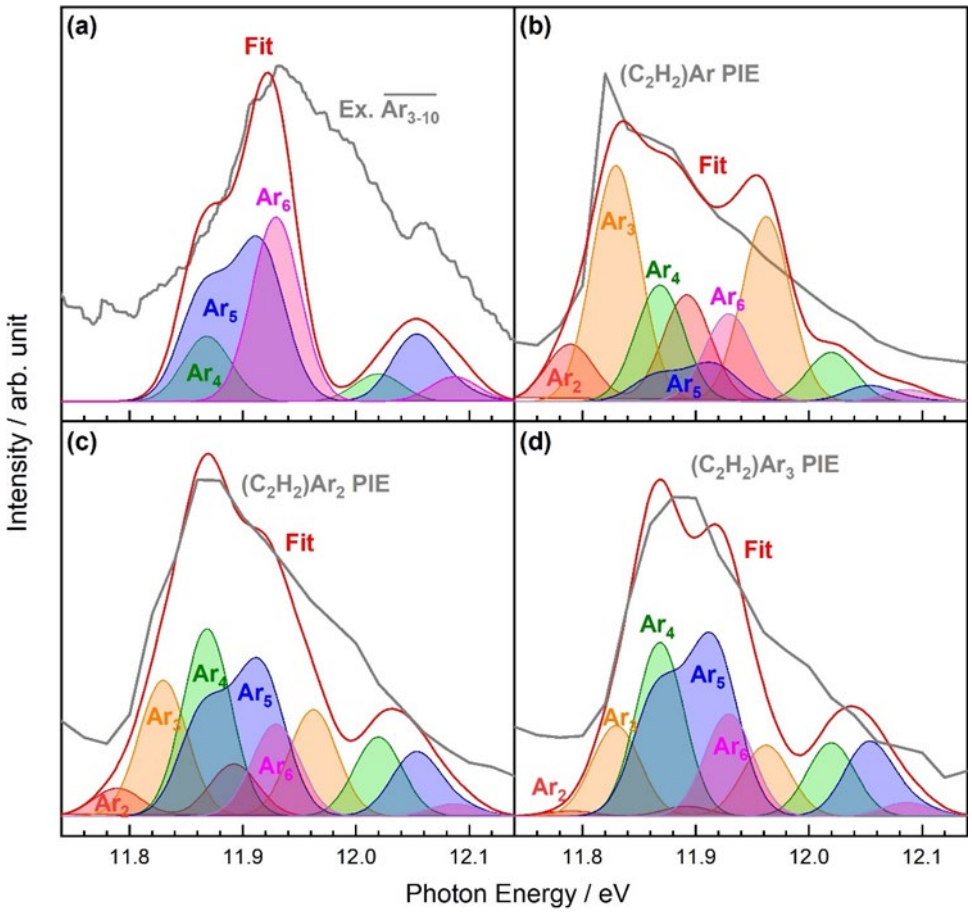

Fig. 5 Fits of the (a) experimental excitation spectra of $\overline{Ar_{3-10}}$, (b) PIE curve of $(C_2H_2)Ar$, (c) PIE curve of $(C_2H_2)Ar_2$, and (d) PIE curve of $(C_2H_2)Ar_3$ using EOM-CCSD calculated Ar_{2-6} excitation spectra in Fig. 3e.

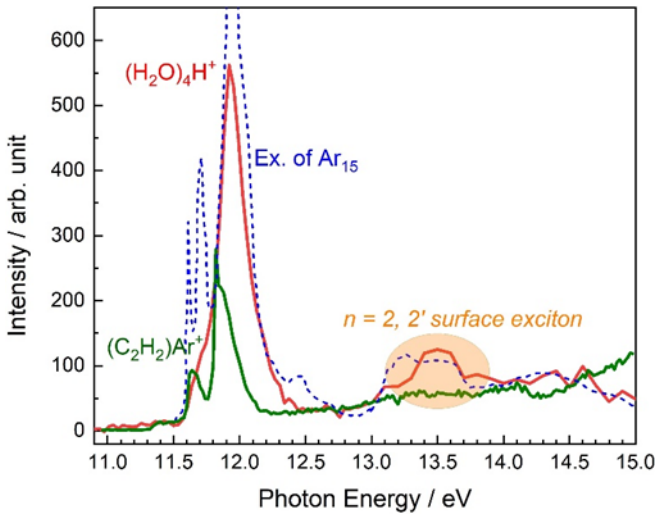

Fig. 6 Comparison of PIE curves of $(H_2O)_4H^+$ (red, from Ref. 20) and $(C_2H_2)Ar^+$ (green) at 0.1% C_2H_2 concentration. The blue dashed curve presents the excitation spectrum of Ar_{15} from Ref. 48. The excitation band around 13.5 eV corresponds to the n = 2 and 2' surface excitons of solid Ar.

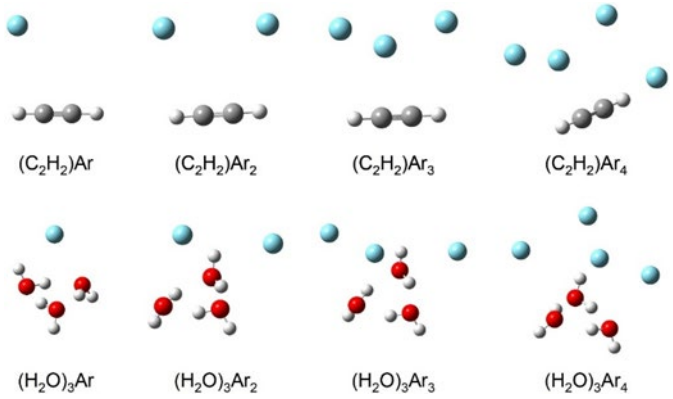

Fig. 7 Global minimum geometries of $(C_2H_2)Ar_n$ and $(H_2O)_3Ar_n$ (n = 1 – 4), calculated at ωB97XD/cc-pVTZ level of theory.